

# Supplementary Information for "Examining 22 Years of Ambient Seismic Wavefield at Mount St. Helens"

Manuela Köpfli , Marine A. Denolle , Weston Thelen , Peter Makus , and Stephen D. Malone

## Contents

<b>Supplementary Table</b>	<b>3</b>
<b>Supplementary Figures</b>	<b>4</b>
Data Quality . . . . .	4
Event Detection . . . . .	5
Seismic Wavefield Analysis . . . . .	6
Comparison of DSAR & VSAR . . . . .	8
Clustering based on Scattering Coefficients . . . . .	9
Z-score Normalization & Feature Time Series . . . . .	12
Tremor . . . . .	15
Seismic Stations sorted by Crater Distance . . . . .	17
Comparison of Lake Level, Borehole Level & DSAR . . . . .	19
<b>1980 Eruption of Mount St. Helens</b>	<b>20</b>

## List of Tables

1	Seismic stations in a radius of 18 km of Mount St. Helens. . . . .	3
2	Different frequency bands and ratios. . . . .	3

## List of Figures

1	Seismic Station Issues. . . . .	4
2	Detected seismic events per 10 minutes. . . . .	5
3	Comparison of DSAR with spectral width. . . . .	6
4	Comparison of DSAR with RSAM. . . . .	7
5	Power Spectral Density (PSD) of the ambient wavefield. . . . .	7
6	Comparison of Displacement Seismic Amplitude Ratio (DSAR) and Velocity Seismic Amplitude Ratio (VSAR). . . . .	8
7	Displacement Seismic Amplitude Ratio (DSAR) and Velocity Seismic Amplitude Ratio (VSAR) are proportional. . . . .	8
8	Elbow curve. . . . .	9
9	Dendrogram showing the distance between the clusters in feature space. . . . .	9
10	Bar plot showing the number of time windows within a cluster. . . . .	10
11	Cluster activity during eruption onset. . . . .	10
12	Example waveforms of station SHW for each cluster. . . . .	11
13	Z-score normalization of the onset of the 2004 eruption. . . . .	12
14	Z-score normalization of 22 years of seismic wavefield data products. . . . .	13
15	22 years of seismic wavefield data products. . . . .	14
16	Tremor occurring on the 3rd October at 9:50 UTC. . . . .	15
17	Gliding Tremor. . . . .	16
18	RSAM 2-5 Hz time series sorted by station-crater distance. . . . .	17
19	RSAM 4.5-8 Hz time series sorted by station-crater distance. . . . .	17
20	RSAM 8-16 Hz time series sorted by station-crater distance. . . . .	18
21	DSAR time series sorted by station-crater distance. . . . .	18
22	Comparison of Water Level, Snow Height, and Seismic Wavefield Attenuation (DSAR). . . . .	19
23	Onset of the 1980 eruption. . . . .	20

## Supplementary Table

**Table S1: Seismic stations in a radius of 18 km of Mount St. Helens.** The stations listed below are mainly sorted by the seismic network [University of Washington, 1963, Cascades Volcano Observatory/USGS, 2001]. Some seismic instruments switched the network during the period of interest between 2000 and 2022. Our study only uses seismometers within 18 km of Mount St. Helens' crater. We only use the vertical (Z) component because most UW-network stations only have a vertical component.

Network	Station	Channel
UW	EDM	EHZ
UW	SHW	EHZ
UW	HSR	EHZ
UW	SOS	EHZ
UW	JUN	EHZ
UW	ELK	EHZ
UW	TDL	EHZ
UW	SUG	EHZ
UW	YEL	EHZ
UW	FL2	EHZ
UW	CDF	EHZ
UW	SEP	EHZ
CC	SEP	EHZ
UW	STD	EHZ
CC	STD	BHZ
CC	VALT	BHZ
CC	JOR	BHZ
CC	HOA	BHZ
CC	LOO	BHZ
CC	USFR	BHZ
CC	NED	EHZ
CC	REM	BHZ
CC	SWFL	BHZ
CC	SFW2	BHZ
CC	MIDE	BHZ
CC	MIBL	EHZ
CC	BLIS	EHZ
CC	RAFT	EHZ
CC	SPN5	EHZ
CC	SEND	EHZ

**Table S2: Different frequency bands and ratios.** The table below explains the naming convention for the different Displacement Seismic Amplitude Ratios (DSAR) used as well as for the analog of DSAR, Velocity Seismic Amplitude Ratio (VSAR). For the Real-time Seismic Amplitude Measurement (RSAM), the used frequency bands are specified.

RSAM	DSAR	VSAR
2 – 5 Hz	IDSAR $\frac{2-5 \text{ Hz}}{4.5-8 \text{ Hz}}$	-
4.5 – 8 Hz	lhDSAR $\frac{2-5 \text{ Hz}}{8-16 \text{ Hz}}$	-
8 – 16 Hz	DSAR $\frac{4.5-8 \text{ Hz}}{8-16 \text{ Hz}}$	$\frac{4.5-8 \text{ Hz}}{8-16 \text{ Hz}}$

## Supplementary Figures

### Data Quality

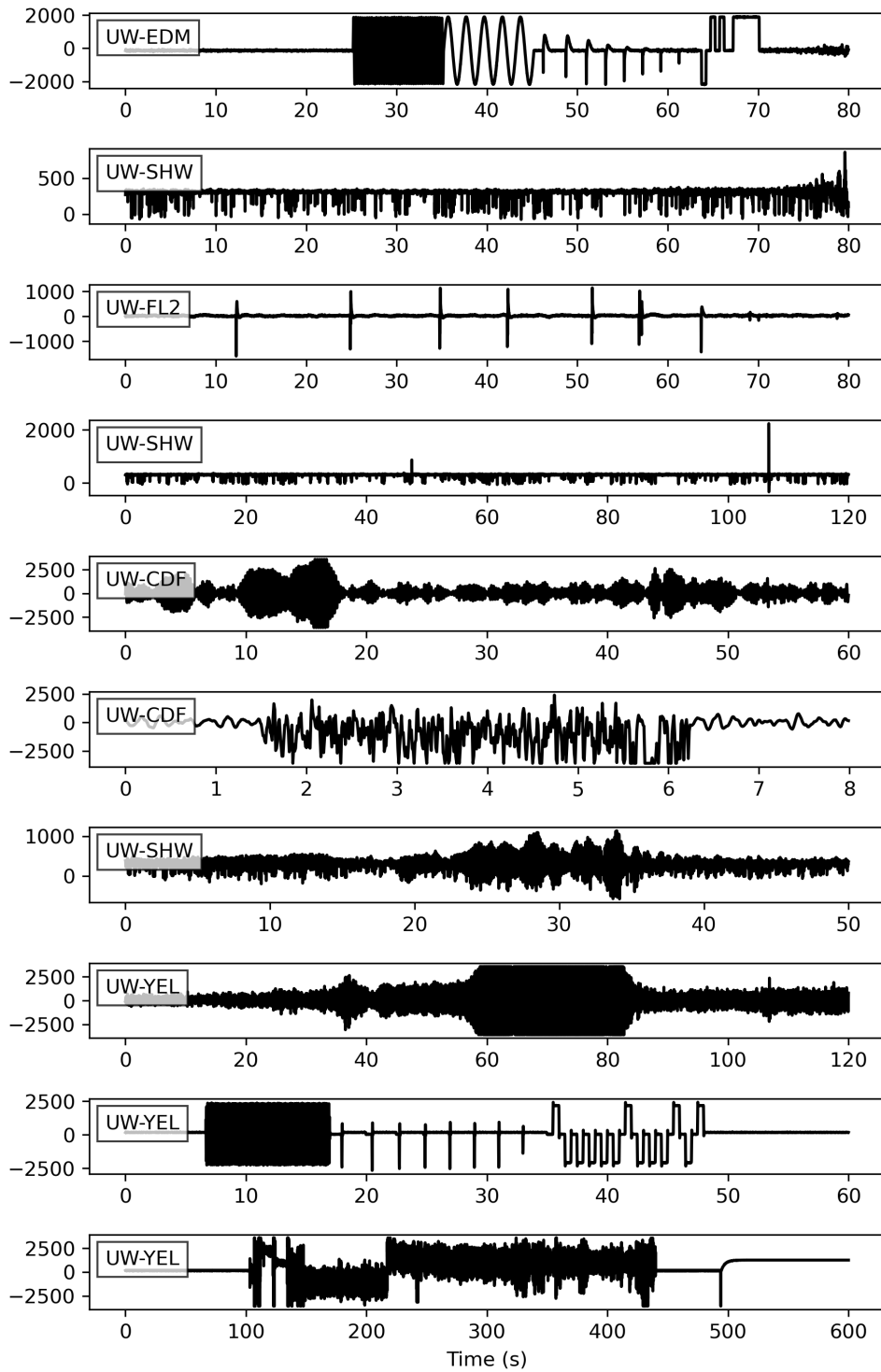


**Figure S1: Seismic Station Issues.** The seismogram illustrates a specific time interval in seconds during which a seismic station, network, and station code in the upper left corner fails to accurately record ground velocity. The diverse nature of these issues poses challenges in their systematic removal or filtering. Consequently, we initially proceed with calculations, temporarily overlooking these problems. However, instances where a problem dominates a specific time window or simultaneous occurrences across different stations can lead to its amplification, potentially influencing the analysis results. To mitigate the risk of misinterpreting issues as natural seismic events or processes, a thorough manual check of the raw data is conducted before the interpretation of time series data.

## Event Detection

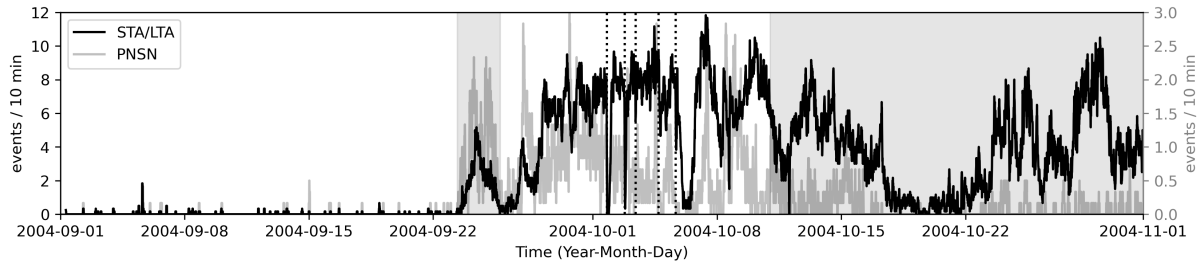


**Figure S2: Detected seismic events per 10 minutes.** The black line represents the events detected by a classic STA/LTA coincidence trigger (short window: 0.5 s, long window: 30 s, trigger on: 5.5 and trigger off: 1) and 50% of the available stations have to trigger at the same time. The gray line represents the events in the Mount St. Helens region in the PNSN catalog. The vertical dotted lines represent the timing of explosions and tremors. The first gray period shows the shallow earthquake swarm, while the second shows the dome growing period.

## Seismic Wavefield Analysis

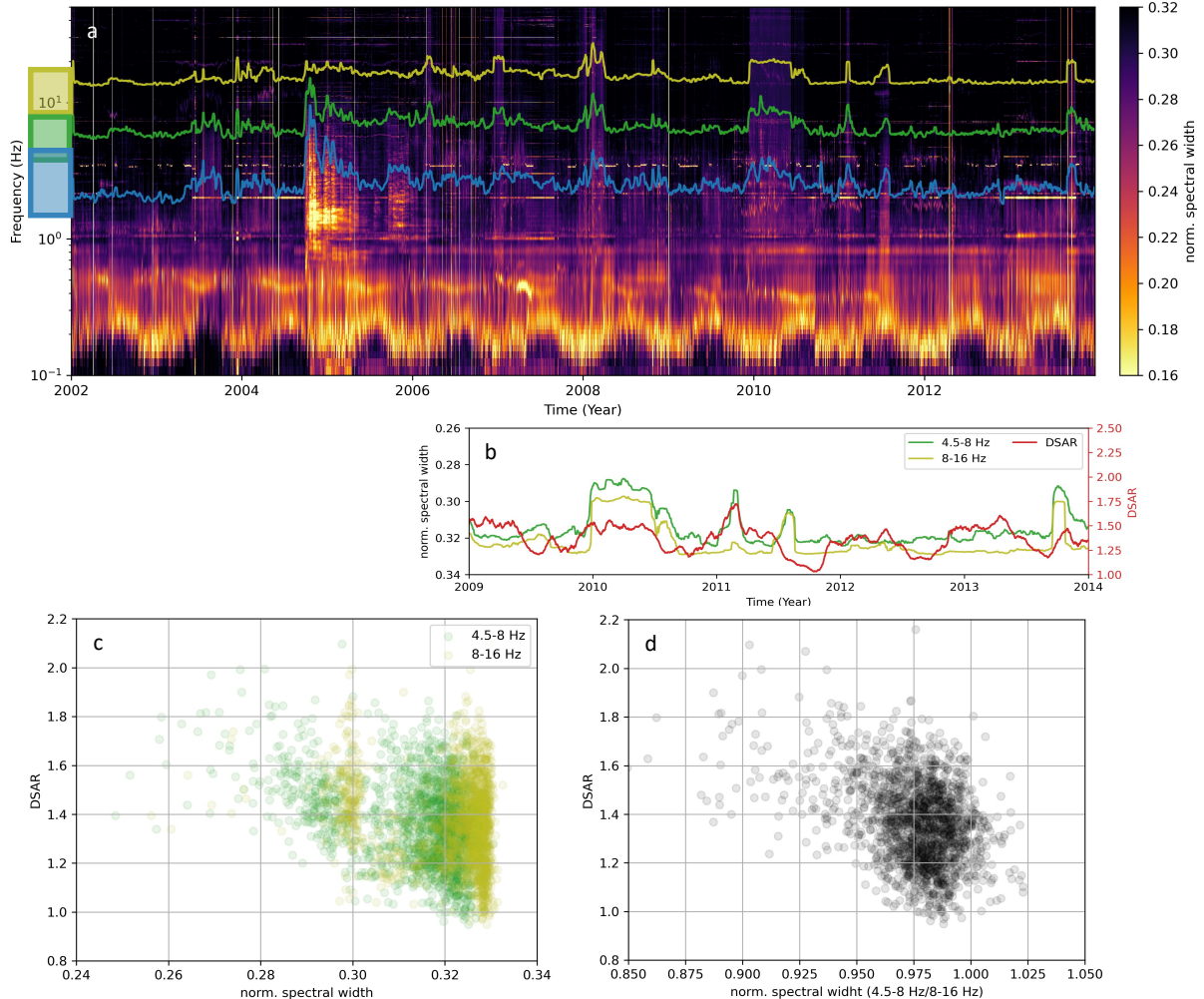


**Figure S3: Comparison of DSAR with spectral width.** a) Spectral width series starting after the volcanic eruption to analyze the seismic wavefield. Frequency bands relevant to this study: 2-5 Hz (blue), 4.5-8 Hz (green), and 8-16 Hz (yellow). b) The two spectral width frequency bands (4.5-8 Hz and 8-16 Hz) used for DSAR show no seasonal signal. c,d) The relation between spectral width and DSAR does not show a significant correlation. This allows us to interpret DSAR as a structural measure independent of changing seismic sources after the eruption.

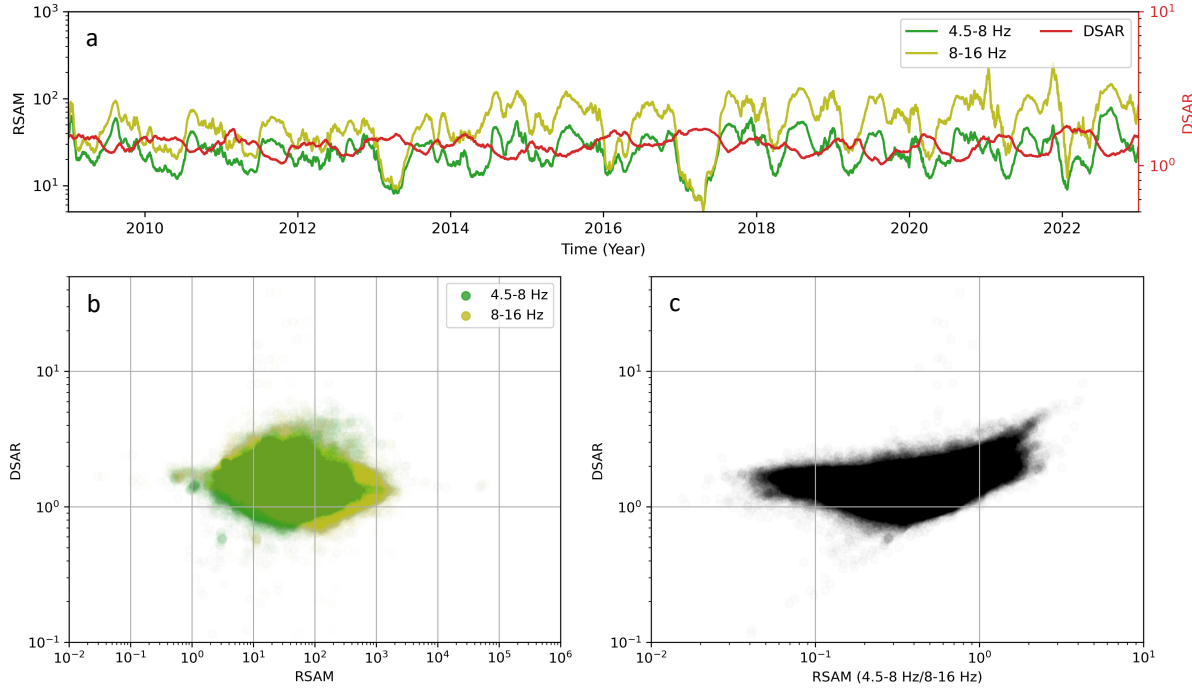


**Figure S4: Comparison of DSAR with RSAM.** (a) RSAM and DSAR time series starting after the volcanic eruption to analyze the seismic wavefield. The two RSAM frequency bands (4.5-8 Hz and 8-16 Hz) used for DSAR show a seasonal signal. Although the RSAM time series changed slightly around 2015, the DSAR signal did not change. b) The relation between RSAM and DSAR and c) RSAM (4.5-8 Hz / 8-16 Hz) does not show a significant correlation between RSAM and DSAR. This allows us to interpret DSAR as a structural measure after the eruption.

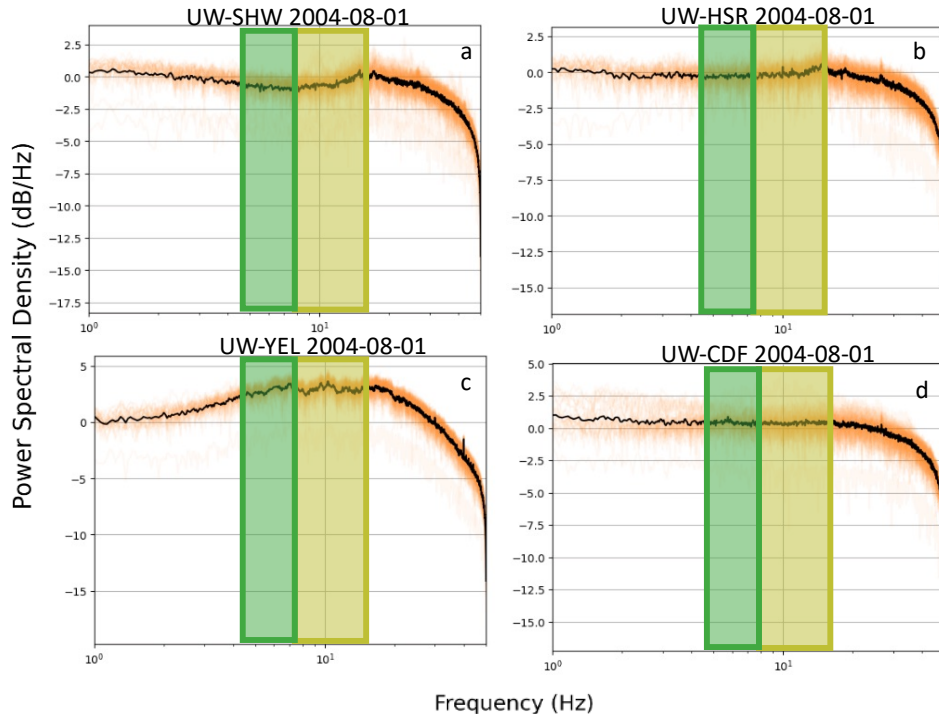


**Figure S5: Power Spectral Density (PSD) of the ambient wavefield.** The four subplots represent the ambient wavefield on August 1st, 2004 (two months before the eruption onset). The green frequencies are used to calculate DSAR. Each subplot shows the wavefield at a different location: a) SHW, b) HSR, c) YEL, and d) CDF. Notice the difference in the noise floor at different locations. The thin orange lines are PSDs of individual time windows, where the black line is their mean.

## Comparison of DSAR & VSAR

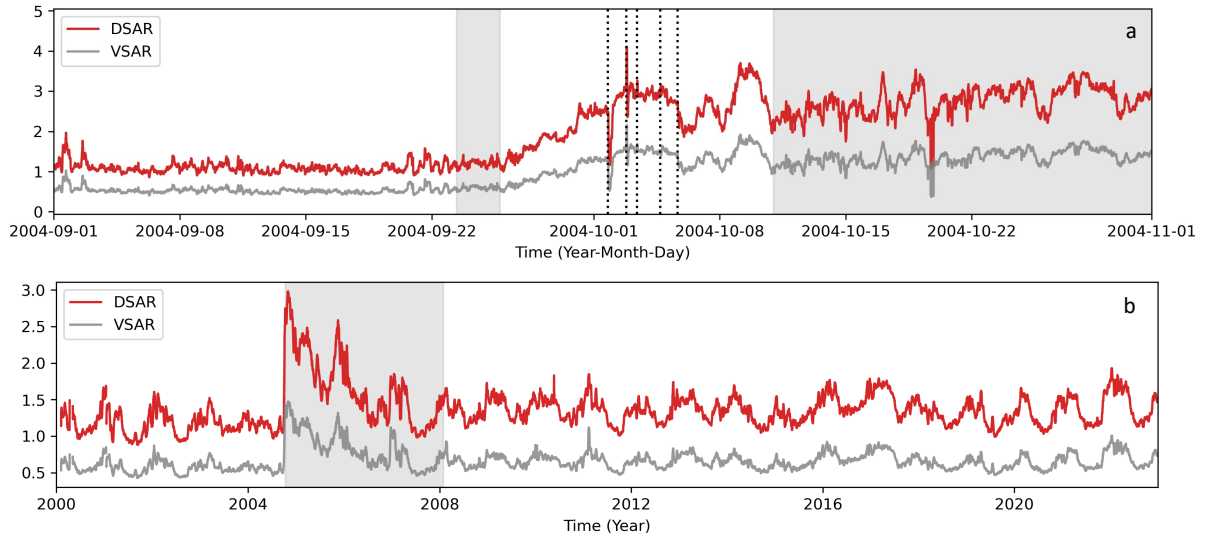


**Figure S6: Comparison of Displacement Seismic Amplitude Ratio (DSAR) and Velocity Seismic Amplitude Ratio (VSAR).** a) Two months at the onset of the eruption where the vertical dotted lines represent the timing of the explosions and tremors. The earthquake swarm and dome growing period are shown in gray. A median rolling over 1 hour is applied to the data. b) 22 years of seismic wavefield with the gray period representing increased volcanic activity. A median rolling over 10 days is applied to the data. Both subplots show a strong correlation between DSAR and VSAR with a slight offset if used as absolute measures. From the similarity of DSAR and VSAR, we infer that the time-integral displacement for DSAR does neither offer additional insights nor does it introduce any artifacts.

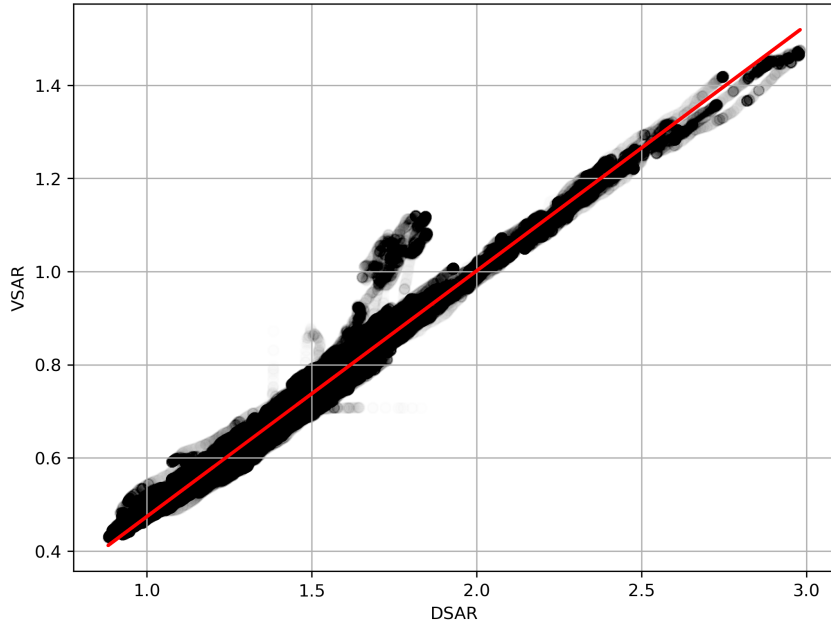


**Figure S7: Displacement Seismic Amplitude Ratio (DSAR) and Velocity Seismic Amplitude Ratio (VSAR) are proportional.** VSAR plotted again, DSAR follows a linear proportionality. The linear regression (red) has a slope of 0.527, an interception of -0.053, and a  $R^2$ -value of 0.976. A median rolling over 10 days is applied to the data.

## Clustering based on Scattering Coefficients

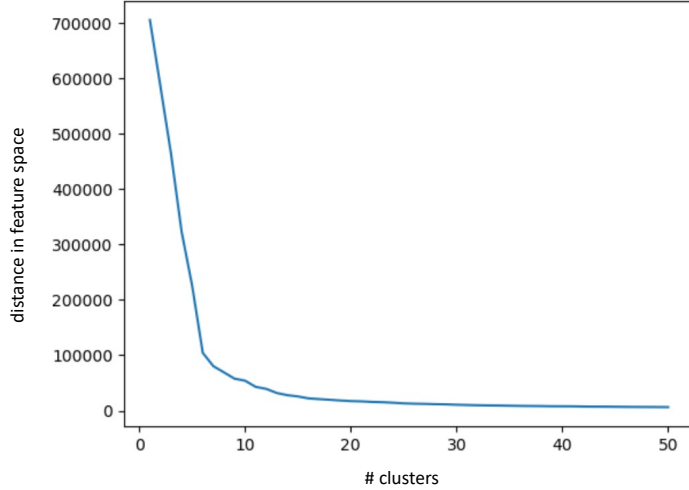


**Figure S8: Elbow curve.** The elbow curve relates the distance between time windows and the center of its corresponding cluster in feature space (y-axis) for different numbers of built clusters (x-axis). The elbow curve helps to find the optimal number of clusters. We allow the algorithm to build 7 clusters based on the elbow curve shown above.

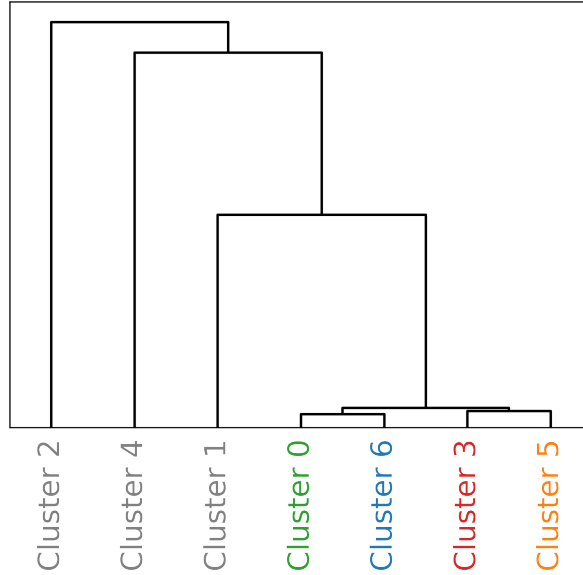


**Figure S9: Dendrogram showing the distance between the clusters in feature space.** The three gray clusters on the left lie far away (in the 5D feature space) from the four colored clusters on the right, in the dendrogram represented as long branches. We found that the gray clusters often contain time windows when station problems occur at some stations. The four colored clusters can be split into two groups. The clusters containing background noise (red, orange) are on the right, and the clusters containing events (green, blue) are on the left. This finding is supported by comparing the Power Spectral Density (PSD) and the waveforms of the clusters. In the main text, we ignore data from the three gray clusters.

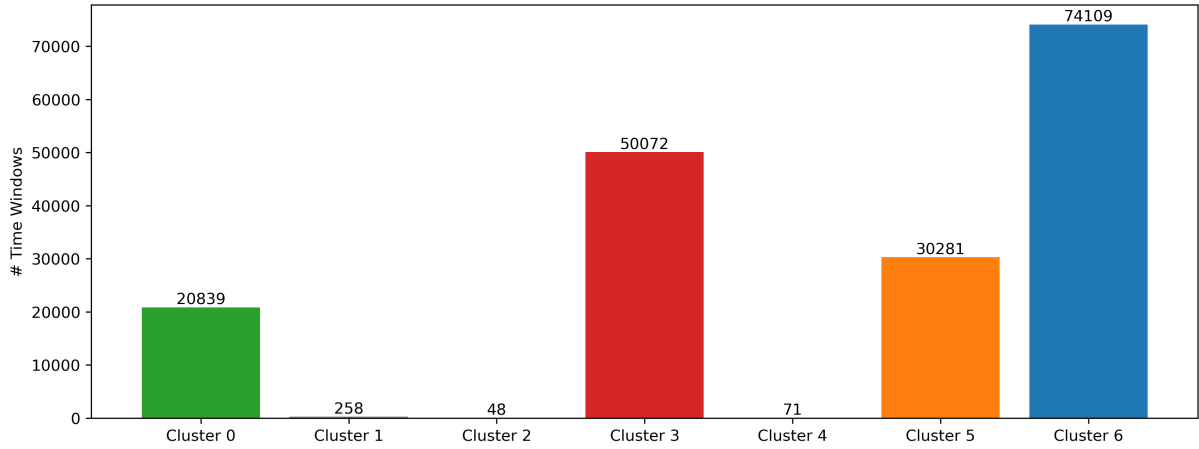


**Figure S10: Bar plot showing the number of time windows within a cluster.** The number of time windows (y-axis) belonging to the respective cluster (x-axis) shows clearly that cluster1, cluster2, and cluster4 are almost empty compared to the other four colored clusters. That is another argument to ignore cluster1, cluster2, and cluster4.

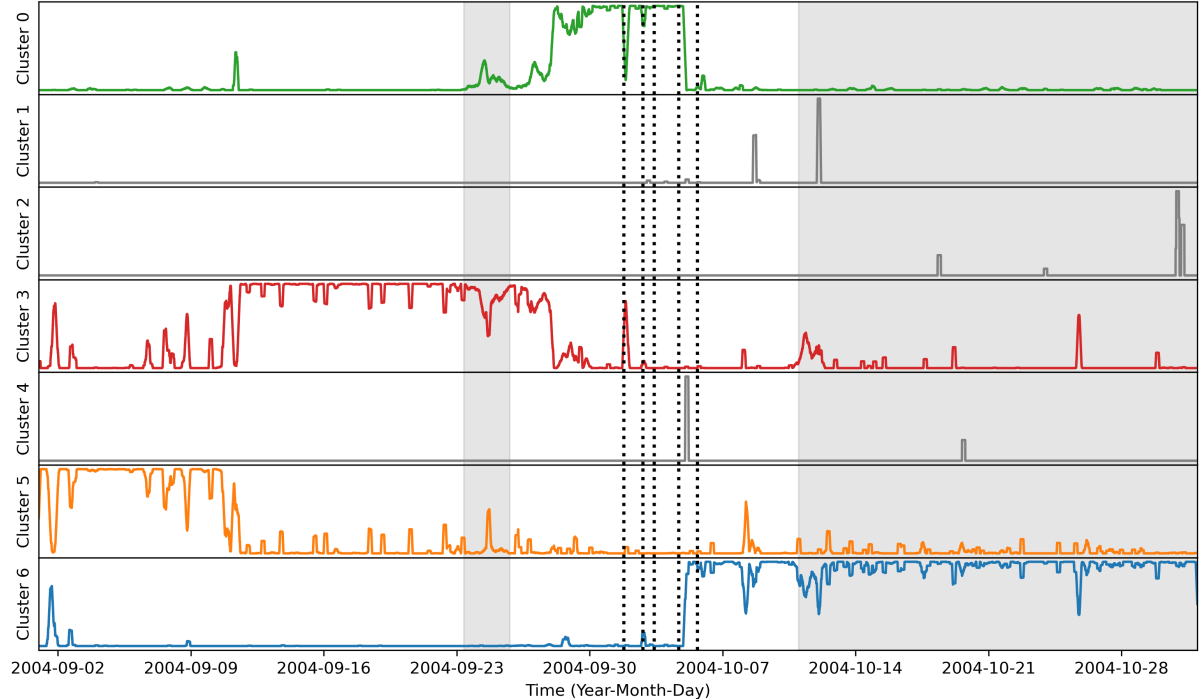


**Figure S11: Cluster activity during eruption onset.** Each subplot represents the activity of a certain cluster smoothed over 4 hours. The main text only considers the colored clusters because of the number of time windows and the position in the feature space. The vertical dotted lines represent the timing of the earthquake swarm, explosions, and tremors, and the dome growing period is shown in gray.

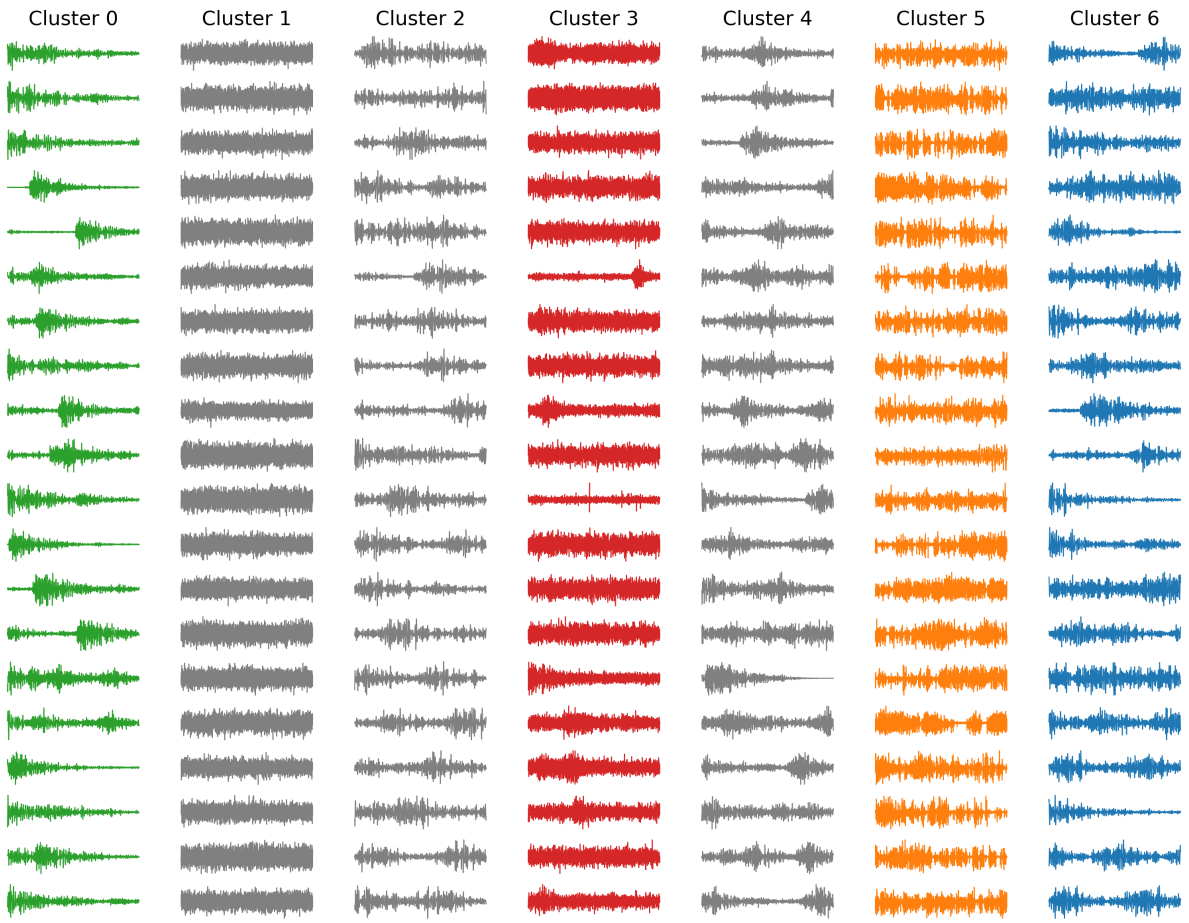


**Figure S12: Example waveforms of station SHW for each cluster.** Each column shows 20-time windows belonging to the cluster labeled on top. All waveforms are collected at station SHW, but the clustering is based on the whole UW network. The gray clusters are neglected in the main text because of the number of time windows and the position in the feature space.

## Z-score Normalization & Feature Time Series

The z-score normalization represents how much the time series changed compared to the past, in our case, the past two days. We apply the z-score normalization in the log space. This specific normalization enhances ongoing changes by comparing the current data to the mean and standard deviation of the past.

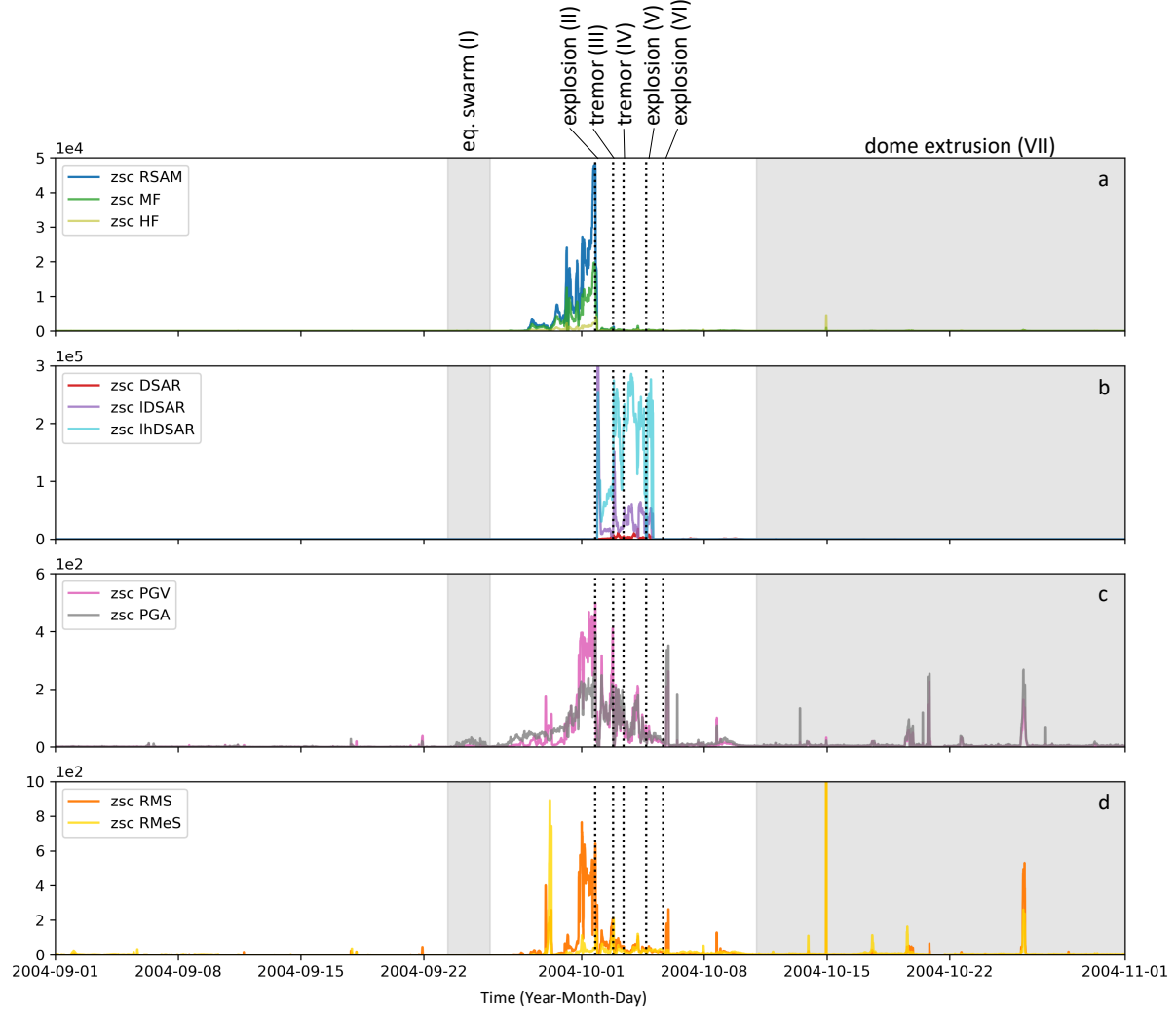


**Figure S13: Z-score normalization of the onset of the 2004 eruption.** In all subplots, the vertical dotted lines represent the timing of the earthquake swarm, explosions, and tremors. The dome growing period is shown in gray. a) Z-score normalized Real-time Seismic Amplitude Measurement indicating changes in emitted seismic power relative to the past two days. Three colors represent different frequency bands (RSAM: 2-5 Hz, MF: 4.5-8 Hz, HF: 8-16 Hz). b) Z-score normalized Displacement Seismic Amplitude Ratio (DSAR: (4.5-8 Hz)/(8-16 Hz), IDSAR: (2-5 Hz)/(4.5-8 Hz), lhDSAR: (2-5 Hz)/(8-16 Hz)) measures changes in wave attenuation relative to the past two days. c) Z-score normalized Peak Ground Velocity (PGV) and Peak Ground Acceleration (PGA) represent maximum absolute ground velocity/acceleration compared to the past two days. d) Z-score normalized Root Mean Square (RMS) and Root Median Square (RMeS) measure unfiltered emitted seismic power relative to the past two days. Z-score normalization reflects changes at time  $t$  compared to  $t - 2$  days. Some measurements, such as RSAM (a) and PGV, PGA (c), detect abnormal seismicity earlier than others (DSAR, (b)), highlighting their potential as better or worse eruption prediction indicators for the eruption at Mount St Helens.

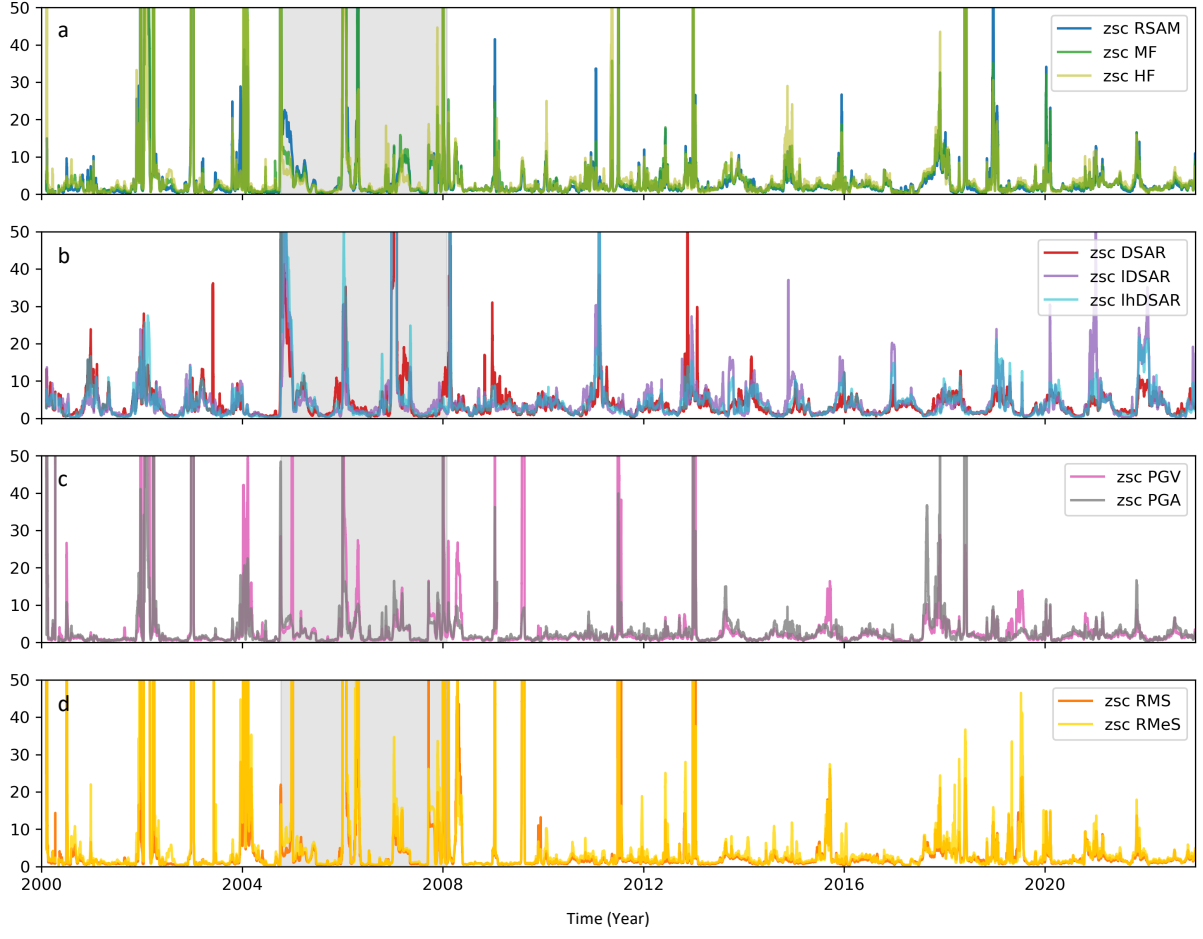


**Figure S14: Z-score normalization of 22 years of seismic wavefield data products.** In all subplots, the gray period represents the period of increased volcanic activity. a) Z-score normalized Real-time Seismic Measurement representing the emitted seismic power relative to the past two days. Three colors represent different frequency bands (RSAM: 2-5 Hz, MF: 4.5-8 Hz, HF: 8-16 Hz). b) Z-score normalized Displacement Seismic Amplitude Ratio (DSAR: (4.5-8 Hz)/(8-16 Hz)), IDSAR: (2-5 Hz)/(4.5-8 Hz), IhDSAR: (2-5 Hz)/(8-16 Hz) measures changes in wave attenuation relative to the past two days. c) Z-score normalized Peak Ground Velocity (PGV) and Peak Ground Acceleration (PGA) represent maximum absolute ground velocity/acceleration compared to the past two days. d) Z-score normalized Root Mean Square (RMS) and Root Median Square (RMeS) measure unfiltered emitted seismic power relative to the past two days. Z-score normalization reflects changes at time  $t$  compared to  $t - 2$  days. We observe the strongest and clearest seasonality in panel (b).

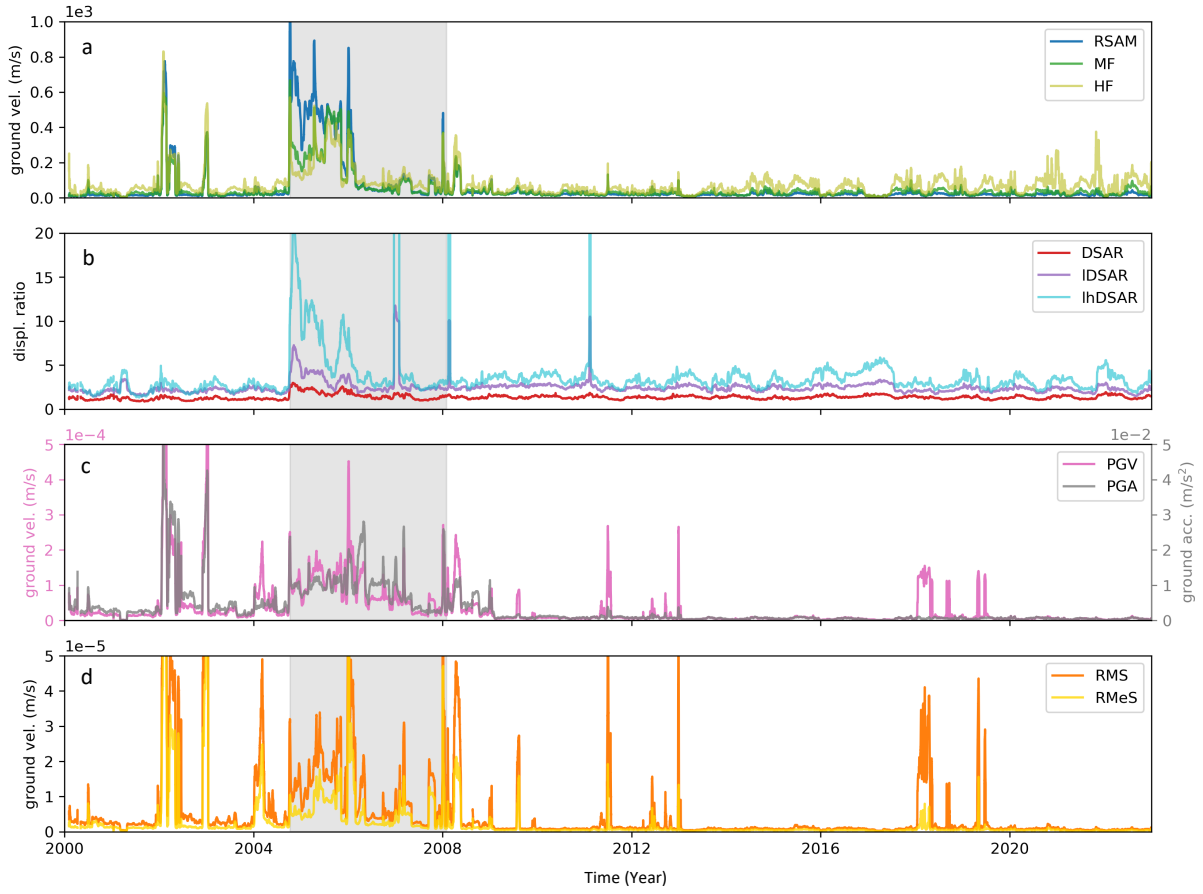


**Figure S15: 22 years of seismic wavefield data products.** In all subplots, the gray period represents the period of increased volcanic activity. a) Real-time Seismic Measurement representing the emitted seismic power in different frequency bands (RSAM: 2-5 Hz, MF: 4.5-8 Hz, HF: 8-16 Hz). b) Displacement Seismic Amplitude Ratio (DSAR: (4.5-8 Hz)/(8-16 Hz), IDSAR: (2-5 Hz)/(4.5-8 Hz), lhDSAR: (2-5 Hz)/(8-16 Hz)) is a measure which is proportional to wave attenuation. c) Peak Ground Velocity (PGV) and Peak Ground Acceleration (PGA) are measurements for the maximum absolute ground velocity/acceleration. d) Root Mean Square (RMS) and Root Median Square (RMeS) are measured from the unfiltered emitted seismic power.

## Tremor

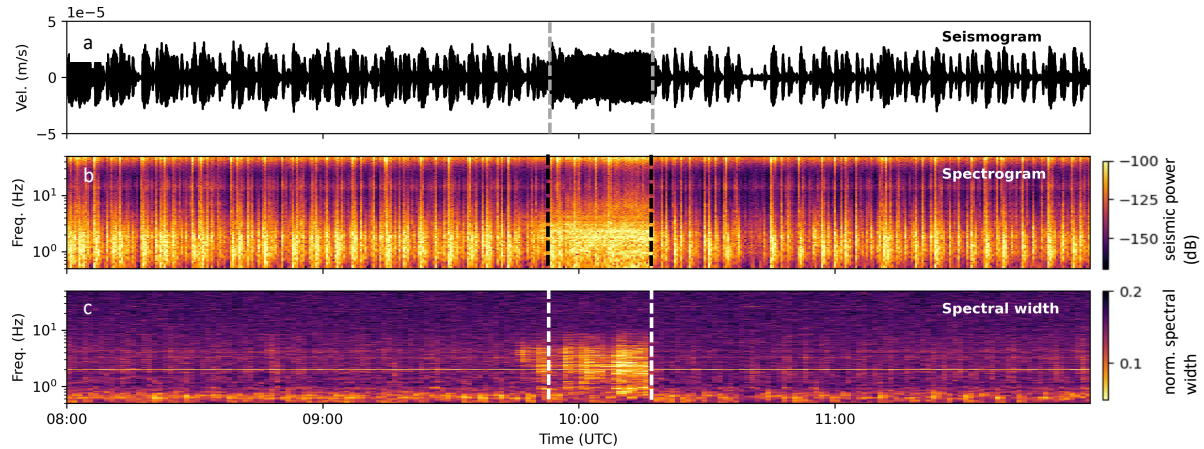


**Figure S16: Tremor occurring on the 3rd October at 9:50 UTC (vertical dashed line) lasting 25 minutes.** a) Seismogram showing 4 hours of station SHW, highpass-filtered above 0.5 Hz and downsampled to 50 Hz. b) Spectrogram representing the same data as (a) without downsampling. Bright colors represent high seismic power. The seismogram (a) and spectrogram (b) show a high low-frequency event rate before the tremor. The tremor itself emits seismic energy continuously in the same frequency range as the distinct events. The tremor is followed by a more quiet period when the distinct events are a bit less frequent. c) Spectral width of 9 stations, but additionally to the instrument correction also, spectral whitening is applied. Bright colors represent a coherent seismic wavefield (low spectral width). The distinct events are suppressed in the spectral width. Therefore, the start and end times of the tremor appear clearer. Compared to the tremor on 2nd October, this time, the tremor onset seems to be a few minutes earlier in the spectral width (c) than the seismogram (a) and spectrogram (b).

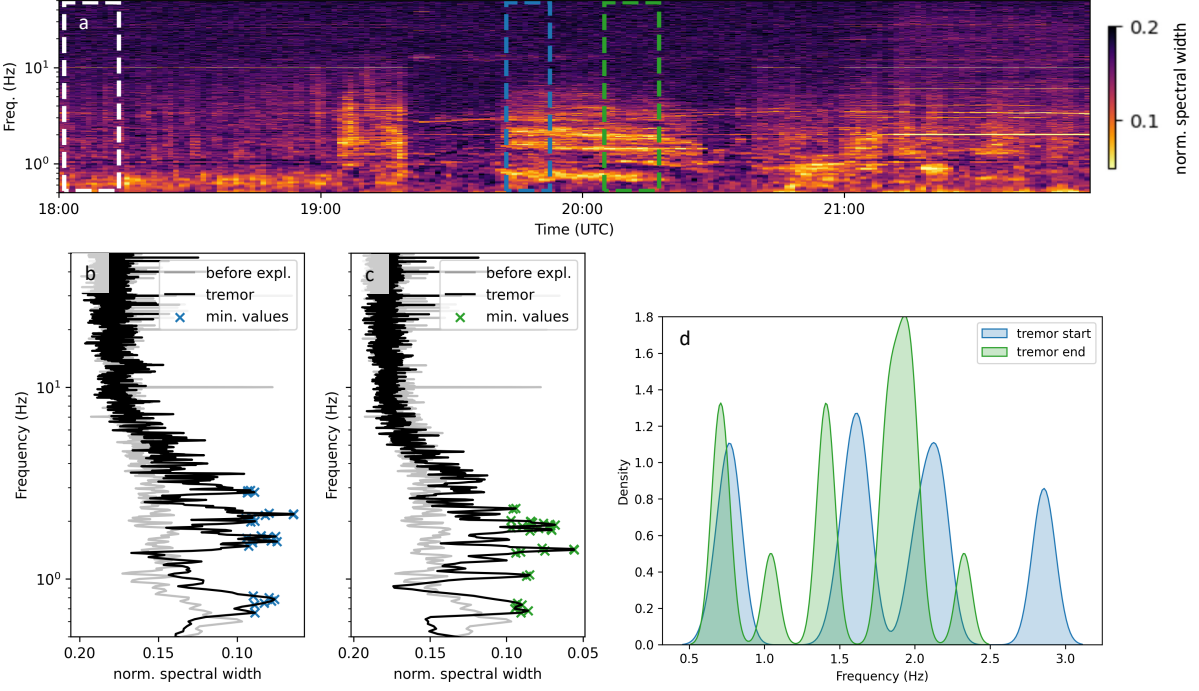


**Figure S17: Gliding Tremor.** a) Spectral width showing a tremor with coherent gliding lines for more than 30 minutes. We pick three 10-minute long time windows: one for reference before the tremor activity starts (white dashed rectangle), one at the tremor onset (blue dashed rectangle), and one at the end of the tremor (green dashed rectangle). The time windows are averaged in time to plot the wavefield coherence (spectral width) as a function of frequency (b) and (c). b) The average spectral width of the reference (white) time is in gray, and the average tremor onset is in black. The crosses mark the 30 smallest values for spectral width (most coherent). c) Same as (b) but for the end of the tremor. d) The density function of the crosses in (b) and (c). Note the slightly shifted frequencies at the end of the tremor (green) compared to the beginning (blue). The most coherent frequencies at the beginning of the tremor period (blue) are 0.76 Hz, 1.60 Hz, 2.10 Hz and 2.86 Hz and for the end of the tremor (green) 0.71 Hz, 1.04 Hz, 1.41 Hz, 1.90 Hz and 2.33 Hz.

## Seismic Stations sorted by Crater Distance

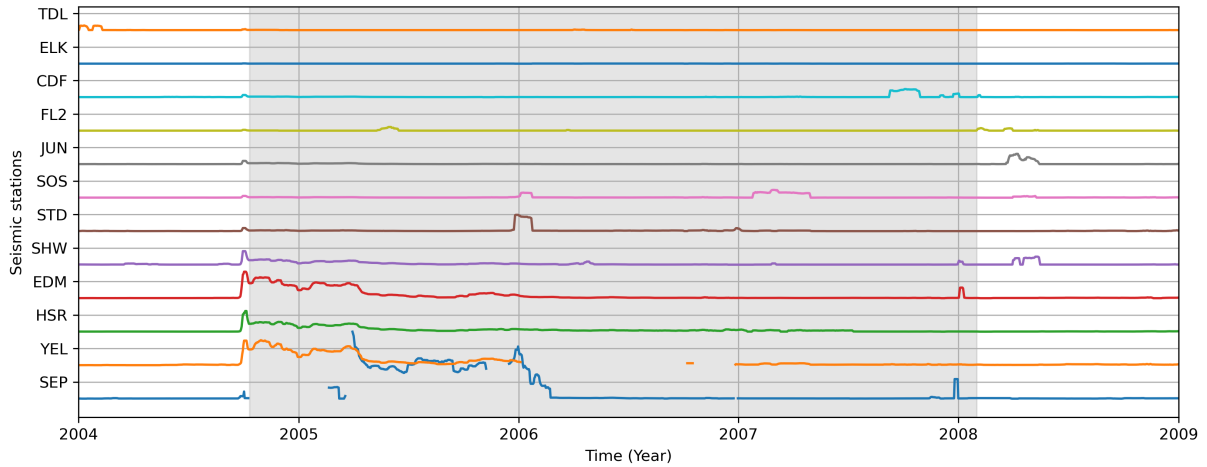


**Figure S18: RSAM 2-5 Hz time series sorted by station-crater distance.** The RSAM time series are sorted so that the station within the crater is the lowest and the further up the further away is the station located from the crater. The time series are normalized so that the max measured value is equal to 1 and the smallest value is equal to 0. Note the side specific amplification at station EDM compared to HSR. Other than the stations SEP to SHW are the stations STD to TDL not at the volcano itself.

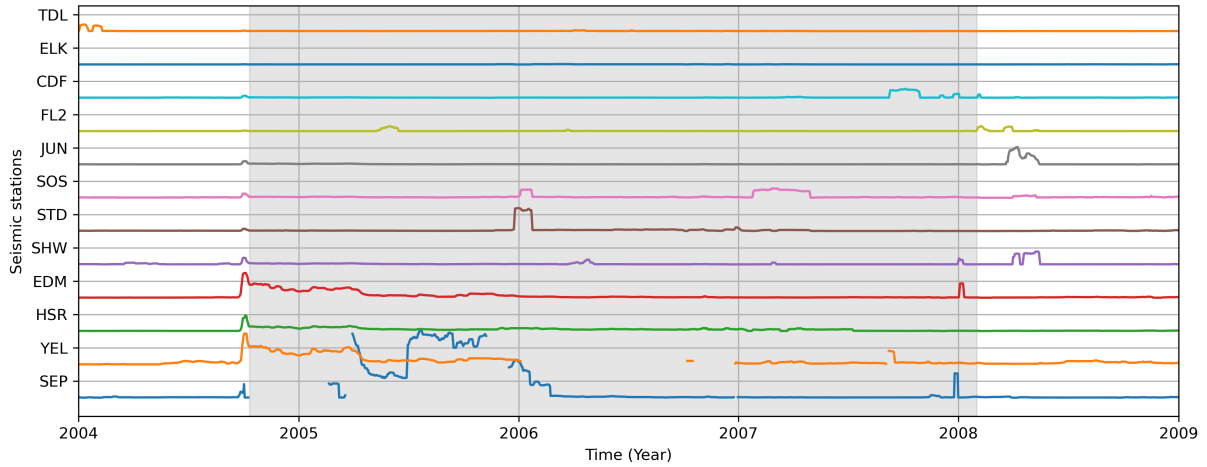


**Figure S19: RSAM 4.5-8 Hz time series sorted by station-crater distance.** The RSAM time series are sorted so that the station within the crater is the lowest and the further up the further away is the station located from the crater. The time series are normalized so that the max measured value is equal to 1 and the smallest value is equal to 0. Note the side specific amplification at station EDM (red) compared to HSR (purple). Other than the stations SEP to SHW are the stations STD to TDL not at the volcano itself.

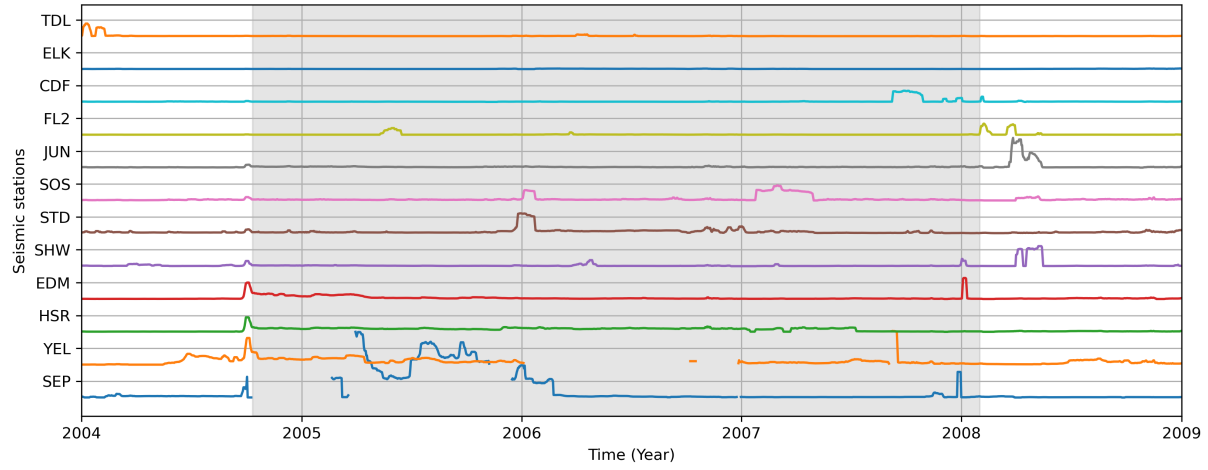


**Figure S20: RSAM 8-16 Hz time series sorted by station-crater distance.** The RSAM time series are sorted so that the station within the crater is the lows and the further up the further away is the station located from the crater. The time series are normalized so that the max measured value is equal to 1 and the smallest value is equal to 0. Note the side specific amplification at station EDM (red) compared to HSR (purple). Other than the stations SEP to SHW are the stations STD to TDL not at the volcano itself.

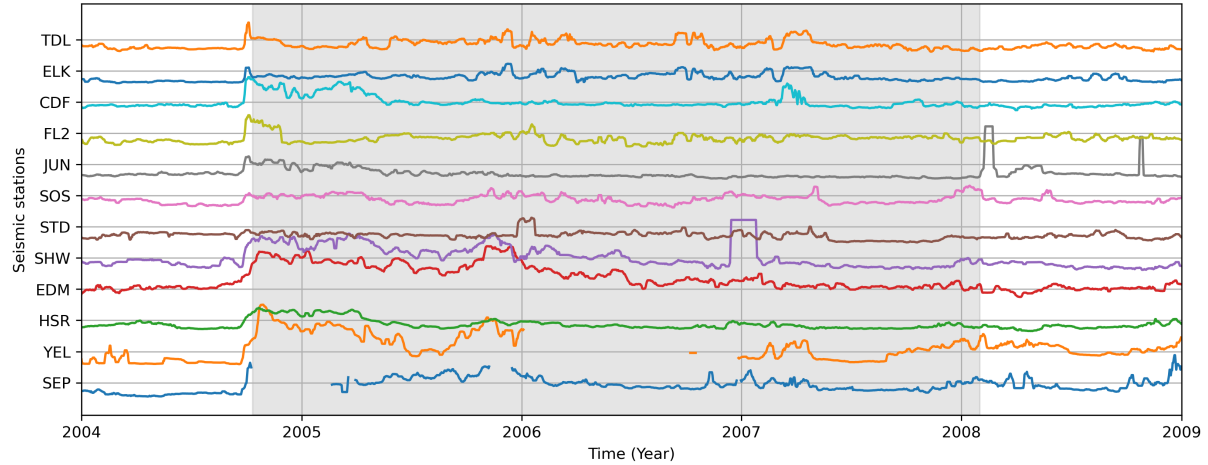


**Figure S21: DSAR time series sorted by station-crater distance.** The DSAR time series are sorted so that the station within the crater is the lows and the further up the further away is the station located from the crater. The time series are normalized so that the max measured value is equal to 1 and the smallest value is equal to 0. Stations STD to TDL are not at the volcano itself leading to almost no increase around 2006 where we observe the second period of high volcanic activity paired with increased DSAR values for the stations at the volcano (SEP-SHW).

## Comparison of Lake Level, Borehole Level & DSAR

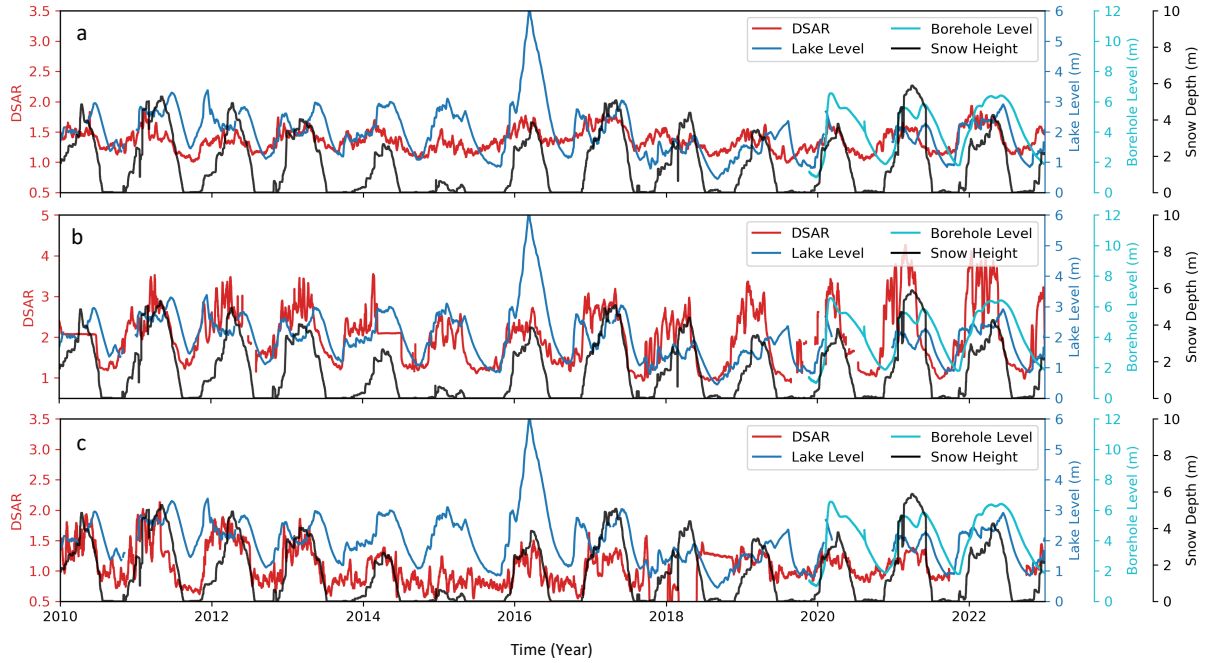


**Figure S22: Comparison of Water Level, Snow Height, and Seismic Wavefield Attenuation (DSAR).** Each subplot displays Spirit Lake's level (blue), borehole water level (light blue), and snow height (black) alongside seismic wave attenuation (DSAR, red) from different stations. a) DSAR represents a stack over the UW network, averaging over a region 18 km around Mount St. Helens with an average elevation of 1450 m.a.s.l. b) DSAR from co-located stations YEL and VALT at the glacier outlet at 1800 m.a.s.l on the north slope of Mount St. Helens. c) DSAR from station SHW at 1500 m.a.s.l on the southwest slope of Mount St. Helens. DSAR in (a) and (b) are shifted 3 months compared to the borehole water level, while DSAR in (c) is almost aligned with the borehole water level. This suggests that the shift between DSAR and the borehole water level may be influenced by the different locations of seismic stations versus the borehole measurement. The lack of or minimal shift observed between the stacked DSAR (a) and the Spirit Lake level supports this interpretation, as both represent more regional measurements. Additionally, we observe a correlation between snow height and DSAR at individual stations (b) and (c), but less so with regional DSAR (a).

## 1980 Eruption of Mount St. Helens

The 1980 dataset consists of 13 vertical-component-only seismometers operated in triggering mode and, thus cannot be used for continuous seismic analysis. There were also five three-component continuous recording seismic stations operated, but only three of these (UW-MUD, UW-APE, UW-CDF) remained active for over a month (25. March 1980 - 21. May 1980). The continuous data collected during the 1980 eruption was initially recorded on magnetic tape and later digitized by Malone [2020]. These magnetic tapes were exchanged every five days. Over the lifetime of the tape, oxide shedding onto the playback head introduced signal interference, leading to a decrease in data quality towards the end of each tape. Notably, the onset of each new tape exhibited comparatively cleaner data with lower noise and higher quality. Tilted instruments were another issue to contend with. However, the most dominant problem, particularly for cross-correlating stations, was the timing discrepancy in the analog data. Timestamps were collected on a separate tape, and temporal misalignment between stations led to several seconds of offset. Regrettably, this timing issue rendered cross-correlation, and consequently spectral width analysis, impractical. As a result, we limited our application of cross-correlation and spectral width analysis to the 2004 eruption period, where data quality and timing alignment were more favorable.

For data digitized from 1980, the removal of instrument response involves additionally the conversion of displacement data into velocity data. It is worth noting that aside from this specific conversion, the procedural framework remains identical for both the 2004 and 1980 datasets.

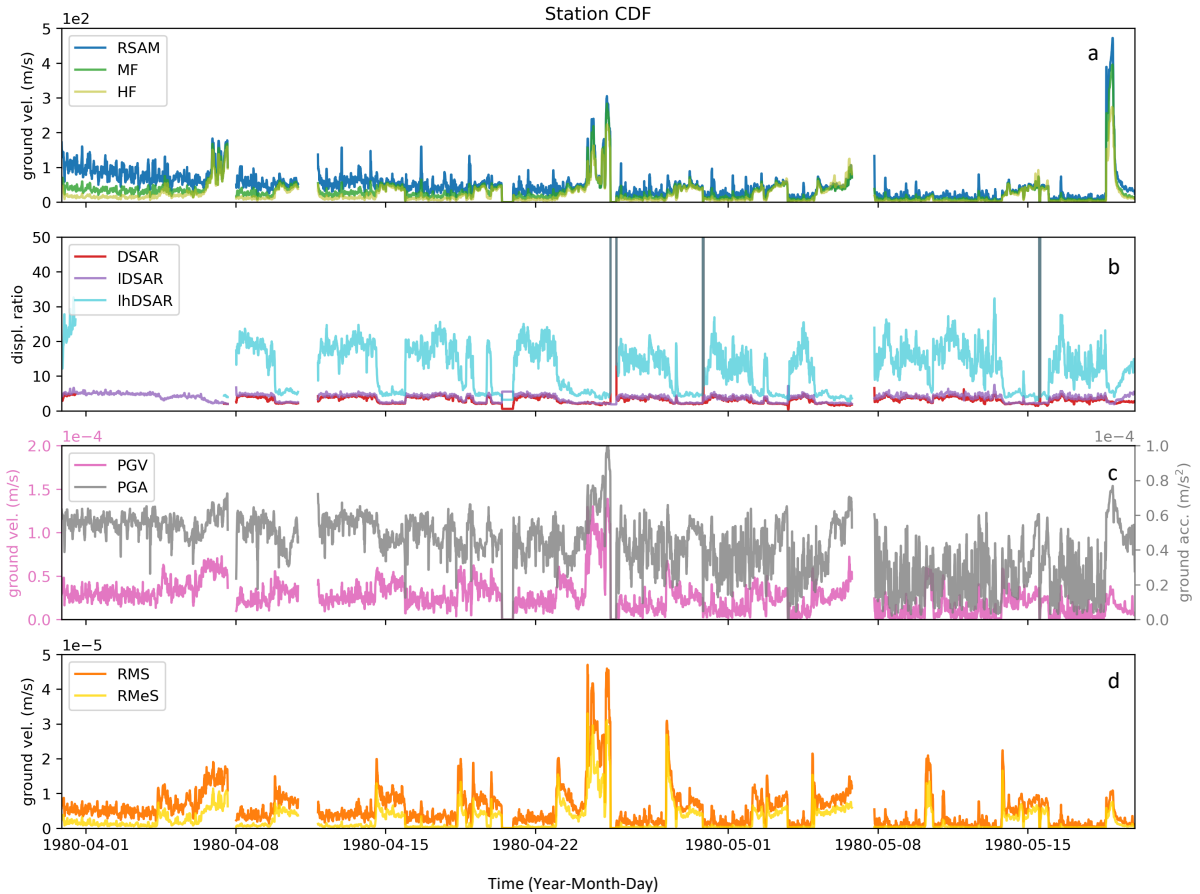


**Figure S23: Onset of the 1980 eruption.** Different from the corresponding figures for 2004, this figure shows time series from a single station CDF. a) Real-time Seismic Amplitude Measurement representing the emitted seismic power in different frequency bands (RSAM: 2-5 Hz, MF: 4.5-8 Hz, HF: 8-16 Hz). b) Displacement Seismic Amplitude Ratio (DSAR: (4.5-8 Hz)/(8-16 Hz), IDSAR: (2-5 Hz)/(4.5-8 Hz), IhDSAR: (2-5 Hz)/(8-16 Hz)) is a measure proportional to seismic attenuation. c) Peak Ground Velocity (PGV) and Peak Ground Acceleration (PGA) are measurements for the maximum absolute ground velocity/acceleration. d) Root Mean Square (RMS) and Root Median Square (RMeS) both measure the unfiltered (broadband) emitted seismic power. In all subplots, the tape exchange and cleaning of the playback head on every fifth day is clearly visible.

## References

- Cascades Volcano Observatory/USGS. Cascade chain volcano monitoring, 2001. URL <https://www.fdsn.org/networks/detail/CC/>.
- Stephen D Malone. Recovering analog-tape seismograms from the 1980 mount st. helens pre-eruption period. *Seismological Research Letters*, 91(3):1430–1440, 2020. doi: 10.1785/0220190327.
- University of Washington. Pacific northwest seismic network - university of washington, 1963. URL <https://www.fdsn.org/networks/detail/UW/>.